Inelastic current–voltage spectroscopy of atomic wires

2003 J. Phys.: Condens. Matter 15 731

(http://iopscience.iop.org/0953-8984/15/4/312)

INSTITUTE OF PHYSICS PUBLISHING JOURNAL OF PHYSICS: CONDENSED MATTER

J. Phys.: Condens. Matter **15** (2003) 731–742 PII: S0953-8984(03)55441-8

Inelastic current–voltage spectroscopy of atomic wires

M J Montgomery[1], J Hoekstra[1], T N Todorov[1] and A P Sutton[2]

[1] School of Mathematics and Physics, Queen's University of Belfast, Belfast BT7 1NN, UK
[2] Department of Materials, University of Oxford, Parks Road, Oxford OX1 3PH, UK

Received 31 October 2002
Published 20 January 2003
Online at stacks.iop.org/JPhysCM/15/731

Abstract

A tight-binding model is developed to describe the electron–phonon coupling in atomic wires under an applied voltage and to model their inelastic current–voltage spectroscopy. Particular longitudinal phonons are found to have greatly enhanced coupling to the electronic states of the system. This leads to a large drop in differential conductance at threshold energies associated with these phonons. It is found that with increasing tension these energies decrease, while the size of the conductance drops increases, in agreement with experiment.

1. Introduction

Point-contact spectroscopy [1] is a technique that allows one to probe the phonon structure of small metallic contacts through electrical measurements. In essence, the technique works as follows. The current through the system is recorded as a function of applied voltage. As the voltage reaches the energies of individual phonon modes, electrons become able to excite these modes by losing energy to them. As each such inelastic electron–phonon scattering mechanism is activated, with increasing voltage, the differential resistance of the contact increases, mapping out the phonon bandstructure.

Recently, there has been interest, both experimentally and theoretically, in the mechanical and electrical properties of metallic atomic chains. Theoretically, current-induced forces [2] and local power dissipation [3] in such systems have been studied. In [3] electron–phonon coupling is modelled by treating the atomic vibrations as Einstein independent oscillators. In this paper, we generalize the formalism to allow electrons to couple to the full, extended phonon modes of a nanojunction. The formalism is implemented in a tight-binding model [4, 5], developed earlier to describe simultaneously mechanical properties and electrical conduction in nanojunctions made of simple metals. The inelastic current–voltage spectra of Au atomic chains between two electrodes are calculated, as a function of tension. The results are compared with experiment [6, 7].

We find that the bond strengths, as quantified by the corresponding dynamical response matrix elements, exhibit great variations down the chain. As a consequence, at least in chains with lengths up to a few atoms, phonons are not free waves, but rather quasi-bound vibrations in subsections of the chain. Electrons couple preferentially to two particular types of longitudinal

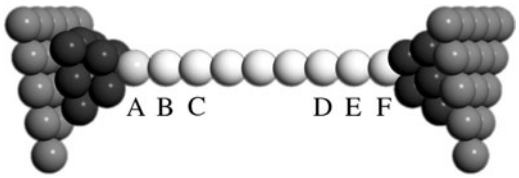

Figure 1. The set-up considered in the paper. The details are discussed in the text.

chain phonon, resulting in clearly defined features in the inelastic current–voltage curves. Tension affects both the voltages at which these features occur, and the magnitude of the features.

2. Method

The system that we consider is shown in figure 1. We have an atomic chain, connected via two dome-shaped contacts to semi-infinite metallic electrodes. The contact atoms are shown as darker circles, for clarity. The electrodes have an fcc crystal structure with a (111) surface. In figure 1 the chain contains nine atoms. Each dome-shaped contact is made of two fcc (111) layers of atoms. The layer adjoining the chain contains three atoms and the layer adjoining the electrode contains six atoms.

This system is described by a self-consistent single-orbital tight-binding model, fitted to the cohesive energy and lattice parameter of bulk Au [5]. This model gives an excellent description of the elastic properties of bulk Au [5]. For a linear Au chain the model gives an equilibrium bond length and a cohesive energy that agree with density functional calculations [2]. Finally, for a linear Au chain the model predicts an ultimate tensile strength [2] that agrees both with density functional calculations and with experiment [8].

The calculations in the paper consist broadly of two parts. In the first part we calculate the phonon modes for a given structure. In the second, we calculate the electron–phonon coupling and its effect on the differential conductance of the structure.

2.1. Phonon modes

The calculation of the phonon modes starts with a relaxation of the geometry for a given separation between the electrodes. At the applied voltages of interest here, of the order of tens of millivolts, the largest current-induced forces in the junction would be of the order of 10^{-3} eV Å^{-1} [2]. Therefore, we ignore any effects of the current on the actual nature of the phonon modes, and the relaxation is carried out at zero current. In this paper only the chain atoms and the contact atoms are allowed to relax, but in principle arbitrarily large sections of each electrode, adjoining the junction, may be included in the relaxation. The calculation of the tight-binding electron Green function, electron density matrix and interatomic forces in the electrode–junction–electrode system is described in [4]. Once the relaxation is complete, the tension in the system may be obtained directly as the total force exerted on either electrode by the rest of the system.

The next step is to calculate the dynamical response matrix. In principle, because the electrode–junction–electrode system is infinite, this matrix is of infinite rank. However, in the present calculations we consider explicitly only the elements of the full dynamical matrix which connect relaxed atoms. These matrix elements form a finite matrix, $\boldsymbol{K}$, with discrete eigenvalues. Like the set of relaxed atoms, the size of $\boldsymbol{K}$ can be made arbitrarily large, without

any change to the formalism below. Further comments on this point will be made later in the paper. The matrix elements of $\boldsymbol{K}$ are computed by displacing each of the relaxed atoms from its equilibrium position and calculating the resultant force on each of the other relaxed atoms. Thus, if atom m is displaced in direction μ by an amount $\delta R_{m\mu}$ and this induces a force $\delta F_{n\nu}$ on atom n in direction ν, then this defines the dynamical matrix element $K_{n\nu m\mu}$ by the equation

$$K_{n\nu m\mu} = -\delta F_{n\nu}/\delta R_{m\mu}. \tag{1}$$

The calculation of $\delta F_{n\nu}$, and hence of the dynamical response matrix $\boldsymbol{K}$ and the resultant phonon modes, discussed below, is done fully self-consistently, within the approximation of local charge neutrality [4, 5].

In principle, the matrix $\boldsymbol{K}$ is symmetric, and hence Hermitian. In practice, errors, such as imperfect relaxation and the use of a finite value for $\delta R_{m\mu}$ in the above equation (in the present calculations $|\delta R_{m\mu}| = 0.005$ Å), result in small asymmetries in $\boldsymbol{K}$. Among the subset of matrix elements of $\boldsymbol{K}$ larger than about 1 eV Å^{-2}, which we could nominally take as being the physically significant ones in the system, the worst asymmetries are of the order of 10%. These asymmetries are removed by setting each of $K_{n\nu m\mu}$ and $K_{m\mu n\nu}$ equal to the average of the two calculated values.

The phonon Hamiltonian for the system may now be written as

$$H_z = \sum_{n,\nu} p_{n\nu}^2/2M_n + \sum_{n,\nu,m,\mu} u_{n\nu} K_{n\nu m\mu} u_{m\mu}/2. \tag{2}$$

Here, $u_{n\nu}$ and $p_{n\nu}$ are the displacement and momentum of atom n in direction ν. M_n is the mass of the atom. In the present case all atomic masses are the same, $M_n = M$, and equal to that of the Au atom. If the atomic masses are not the same, then the formalism may be reduced to the present one by making the scaling transformations $p'_{n\nu} = p_{n\nu}/\sqrt{M_n}$, $u'_{n\nu} = u_{n\nu}\sqrt{M_n}$, $K'_{n\nu m\mu} = K_{n\nu m\mu}/\sqrt{M_n M_m}$. In terms of the primed quantities the formalism is then equivalent to the present one with M equal to the unit mass.

The phonons are quantized by imposing

$$[u_{m\mu},\, p_{n\nu}] = \mathrm{i}\hbar\delta_{mn}\delta_{\mu\nu}. \tag{3}$$

In what follows it will occasionally be convenient to employ a single index, i, instead of the double index $n\nu$, used to label the atomic displacements and momenta, in such a way that there is a unique value of i for every $n\nu$. Let now $\mathcal{M}_{ji}$ be component i of eigenvector j, normalized to unity, of the dynamical matrix, so that

$$\sum_i K_{li}\mathcal{M}_{ji} = K_j\mathcal{M}_{jl} \tag{4}$$

where K_j is the eigenvalue corresponding to eigenvector j. The matrix $\mathcal{M}$ is unitary. In what follows, index j will always be used to label phonon modes. Index j has the same number of values as index $i = n\nu$, used to label the original atomic degrees of freedom. For a given j and a given $i = n\nu$, $\mathcal{M}_{ji}$ gives the normalized amplitude of phonon mode j at atom n, in direction ν. The angular frequency, ω_j, of phonon mode j is given by

$$\omega_j^2 = K_j/M. \tag{5}$$

For a perfectly relaxed, mechanically stable system all K_j must be positive. In practice, a small number of small negative eigenvalues may occur, corresponding to small amounts of residual instability in the system, due to imperfect relaxation. Typically, the number of negative eigenvalues is of the order of one per cent of the total number of eigenvalues, and the magnitude of the largest negative eigenvalue does not exceed one per cent of the largest positive eigenvalue. These artificial modes, as well as the modes with positive eigenvalues of magnitude less than that of the largest negative eigenvalue, are excluded from the rest of the

calculation. The residual instabilities due to imperfect relaxation, and any resultant unphysical modes, mask the lowest-energy true phonon modes of the system. However, none of our central findings on inelastic current–voltage characteristics depend on the lowest-energy modes and we do not consider their exclusion from the calculation significant.

We now introduce the phonon creation and annihilation operators

$$A_j^\dagger = \sum_i \left(\sqrt{M\omega_j/2\hbar}\mathcal{M}_{ji}u_i - \mathrm{i}\sqrt{1/2\hbar M\omega_j}\mathcal{M}_{ji}^* p_i\right) \tag{6}$$

$$A_j = \sum_i \left(\sqrt{M\omega_j/2\hbar}\mathcal{M}_{ji}^* u_i + \mathrm{i}\sqrt{1/2\hbar M\omega_j}\mathcal{M}_{ji} p_i\right) \tag{7}$$

which satisfy $[A_j, A_{j'}] = [A_j^\dagger, A_{j'}^\dagger] = 0$ and $[A_j, A_{j'}^\dagger] = \delta_{jj'}$. The eigenvectors of $\boldsymbol{K}$, and hence the matrix $\mathcal{M}$, may always be chosen to be pure real, but in the notation here we have allowed $\mathcal{M}$ to be a general complex Hermitian matrix. Equations (6) and (7) may be inverted to give

$$u_i = \sum_j \sqrt{\hbar/2M\omega_j}(\mathcal{M}_{ji}A_j + \mathcal{M}_{ji}^* A_j^\dagger) \tag{8}$$

$$p_i = \sum_j \mathrm{i}\sqrt{M\hbar\omega_j/2}(-\mathcal{M}_{ji}A_j + \mathcal{M}_{ji}^* A_j^\dagger). \tag{9}$$

The phonon Hamiltonian may now be expressed in diagonal form as

$$H_z = \sum_j (A_j A_j^\dagger + A_j^\dagger A_j)\hbar\omega_j/2. \tag{10}$$

2.2. Electron–phonon coupling and differential conductance

The electron–phonon interaction is treated perturbatively, in a way similar to that in [3]. In the unperturbed state, every phonon mode is given a degree of thermal excitation defined by the quantity

$$N_j = \langle A_j^\dagger A_j \rangle \tag{11}$$

where the angular brackets designate thermal averaging.

To define the unperturbed state of the electron subsystem, we imagine that the ions are frozen at their equilibrium positions. The electronic structure of the system is described by the same single-orbital tight-binding model as used to calculate the phonon modes above. The electron Hamiltonian is written as

$$H_e = \sum_{m,n} |m\rangle H_{mn}\langle n| \tag{12}$$

where $|n\rangle$ is the tight-binding positional basis state at atomic site n. The electron eigenstates for the electrode–junction–electrode system can be divided into two classes [4, 9, 10]. The states in one class, $\{|\psi_1\rangle\}$ with energies $\{E_1\}$, consist of a right-travelling wave, incident in the left electrode upon the junction, then partially reflected back into the left electrode and partially transmitted into the right electrode, and conversely for the other class, $\{|\psi_2\rangle\}$ with energies $\{E_2\}$. To set up current flow we imagine that a battery of voltage W is connected across the electrodes in figure 1. The battery populates the states $\{|\psi_1\rangle\}$ and $\{|\psi_2\rangle\}$ with Fermi–Dirac occupation functions $f_1(E)$ and $f_2(E) = f_1(E + eW)$, with electrochemical potentials μ_1 and $\mu_2 = \mu_1 - eW$, respectively. Like the calculation of the dynamical matrix and the phonon modes in section 2.1, the calculation of the unperturbed state of the electron subsystem is done self-consistently, within the approximation of local charge neutrality [4, 5, 10]. The variable parameters in the self-consistency are the onsite energies $\{H_{nn}\}$. The intersite Hamiltonian

matrix elements $H_{mn} = H_{nm}$ are functions of the interatomic distance and are parameters of the model [4, 5].

The electronic structure of the current-carrying electrode–junction–electrode system in the absence of electron–phonon interactions is thus described by the density operator

$$\rho(W) = \int f_1(E) D_1(E)\,\mathrm{d}E + \int f_2(E) D_2(E)\,\mathrm{d}E \tag{13}$$

where $D_1(E) = \sum_1 |\psi_1\rangle\delta(E - E_1)\langle\psi_1|$ and $D_2(E) = \sum_2 |\psi_2\rangle\delta(E - E_2)\langle\psi_2|$ are the partial density of states operators associated with the two classes of electron states. Rather than calculating the states $\{|\psi_1\rangle\}$ and $\{|\psi_2\rangle\}$ explicitly, one may use scattering theory [9] to express $D_1(E)$ and $D_2(E)$, and the total density of states operator $D(E) = D_1(E) + D_2(E)$, directly in terms of the Green function for the electrode–junction–electrode system as follows [10, 11]:

$$2\pi\mathrm{i}D_1(E) = P_1G^-(E) - G^+(E)P_1 + G^+(E)(P_2H_\mathrm{e}P_1 - P_1H_\mathrm{e}P_2)G^-(E) \tag{14}$$

$$2\pi\mathrm{i}D_2(E) = P_2G^-(E) - G^+(E)P_2 + G^+(E)(P_1H_\mathrm{e}P_2 - P_2H_\mathrm{e}P_1)G^-(E) \tag{15}$$

$$2\pi\mathrm{i}D(E) = D_1(E) + D_2(E) = G^-(E) - G^+(E). \tag{16}$$

Here, $P_1 = \sum_1 |1\rangle\langle 1|$ and $P_2 = \sum_2 |2\rangle\langle 2|$, where indices 1 and 2 run over all atoms to the left and to the right, respectively, of an arbitrary open surface through the electrode–junction–electrode system [10, 11]. P_1 and P_2 satisfy $P_1 + P_2 = \mathbf{1}$, where $\mathbf{1}$ is the identity operator within the Hilbert space spanned by the orthogonal positional basis $\{|n\rangle\}$. $G^\pm(E)$ are given by $G^\pm(E) = G(E \pm \mathrm{i}\epsilon)$, where ϵ is an infinitesimally small real positive number and $G(z)$ satisfies $(z - H_\mathrm{e})G(z) = G(z)(z - H_\mathrm{e}) = \mathbf{1}$. $G^\pm(E)$ are calculated by a standard numerical procedure, described in [4].

To describe the electron–phonon interaction, we treat the electrons as independent particles and introduce the electron–phonon coupling term

$$V_\mathrm{ez} = \sum_{n,\nu} V_{n\nu}u_{n\nu} \tag{17}$$

where

$$V_{n\nu} = \sum_{m\neq n} (|n\rangle\langle m| + |m\rangle\langle n|)\partial H_{nm}/\partial R_{n\nu}. \tag{18}$$

Here, $\boldsymbol{R_n} = (R_{nx}, R_{ny}, R_{nz})$ is the position of the ion, and the derivative in equation (18) is evaluated with the ions at their equilibrium positions. In terms of the phonon creation and annihilation operators, introduced earlier, V_ez may be expressed as

$$V_\mathrm{ez} = \sum_{i,j} \sqrt{\hbar/2M\omega_j}(\mathcal{M}_{ji}A_j + \mathcal{M}^*_{ji}A^\dagger_j)V_i \tag{19}$$

where we have used the convention $i = n\nu$, introduced earlier, so that V_i in equation (19) is the same as $V_{n\nu}$ in equation (18).

In equation (18), as in our earlier work [3, 12], we have ignored the dynamical self-consistent screening of the electron–phonon interaction. When an atom is displaced, the effective tight-binding electron Hamiltonian changes in two separate ways. First, the hopping integrals change, due to their explicit dependence on the atomic positions. Second, the onsite energies change, due to their self-consistent dependence on the charge redistribution that accompanies atomic motion. This happens in a steady-state Born–Oppenheimer picture [4]. It would happen also in dynamical pictures, such as the non-perturbative time-dependent tight-binding formalism of [13], although of course the actual onsite energy variations in these pictures will not be the same. However, in the present treatment of the electron–phonon interaction we have made a compromise. The electron–phonon coupling term in equations (17)

and (18) includes the bare, unscreened perturbation to the electron Hamiltonian, which arises from the explicit parametric dependence of the hopping integrals on atomic displacements. But the subsequent perturbative calculation, described below, does not include any attempt to describe the dynamical self-consistent additional changes to the electron Hamiltonian that accompany the inelastic electron–phonon scattering.

When the electron–phonon interaction is switched on, two types of process may occur. In one electrons absorb phonons, and in the other electrons emit phonons. Consider processes in which a single quantum is absorbed out of phonon mode j. By standard first-order perturbation theory the total rate of such processes is

$$J_j^- = (4\pi/\hbar)\sum_{\alpha,\beta} N_j f_\alpha(1-f_\beta)|\langle\psi_\beta|\Lambda_j|\psi_\alpha\rangle|^2\delta(E_\beta - E_\alpha - \hbar\omega_j) \tag{20}$$

where a factor of two for electron spin degeneracy has been included and Λ_j is given by

$$\Lambda_j = \sum_i \sqrt{\hbar/2M\omega_j}\mathcal{M}_{ji}V_i. \tag{21}$$

In equation (20), $|\psi_\alpha\rangle$ and $|\psi_\beta\rangle$ each run over all states $\{|\psi_1\rangle\}$ and $\{|\psi_2\rangle\}$, introduced earlier, and $f_\alpha(f_\beta)$ is the occupation of $|\psi_\alpha\rangle(|\psi_\beta\rangle)$. Similarly, the total rate of processes in which a quantum is created in phonon mode j is

$$J_j^+ = (4\pi/\hbar)\sum_{\alpha,\beta}(N_j+1) f_\alpha(1-f_\beta)|\langle\psi_\beta|\Lambda_j^\dagger|\psi_\alpha\rangle|^2\delta(E_\beta - E_\alpha + \hbar\omega_j). \tag{22}$$

This lowest-order perturbative calculation is valid in the limit where the mean time spent by an electron in the nanojunction is smaller than the electron–phonon scattering time therein. This limit may be safely assumed for the systems considered here [3].

As a simplification compatible with experiment [6, 7], we now take the low-temperature limit, in which $N_j \to 0$. That leaves only the second type of process, discussed above. Let us now for definiteness take $eW > 0$, corresponding to an electron particle current from left to right. Using the form of the population functions f_1 and f_2, introduced earlier, invoking the partial density of states operators D_1 and D_2, and ignoring variations in the electron Green function over energies of the order of $\hbar\omega_j$ and eW, for the total inelastically scattered particle current from the class of states $\{|\psi_1\rangle\}$ to the class $\{|\psi_2\rangle\}$ we find

$$\delta J = \sum_j (4\pi e/\hbar)(eW - \hbar\omega_j)\theta(eW - \hbar\omega_j)\,\mathrm{Tr}[D_1\Lambda_j D_2\Lambda_j^\dagger] \tag{23}$$

where θ is the step function, with $\theta(x) = 0$ for $x < 0$, $\theta(x) = 1$ otherwise.

In the limit of weak elastic backscattering, which is the limit of interest here, the change in conductance caused by the inelastic scattering may now be obtained as follows. In the ballistic limit, the states from class $\{|\psi_2\rangle\}$ describe electrons which, once they enter the junction, are fully transmitted into the left electrode. Then the current δJ in equation (23) is the same as the current of incident electrons that are inelastically backscattered into the left electrode. Hence, the inelastic differential conductance is given by

$$\sigma = \sigma_0 - e\,\mathrm{d}\delta J/\mathrm{d}W = \sigma_0 - (e^2/\pi\hbar)\sum_j 4\pi^2\theta(eW - \hbar\omega_j)\,\mathrm{Tr}[D_1\Lambda_j D_2\Lambda_j^\dagger] \tag{24}$$

where σ_0 is the zero-voltage conductance. Here, we have ignored any variations with W in the *elastic* differential conductance, which may be expected to be negligible in nearly ballistic atomic wires, in the voltage range of interest [14].

Equation (24) would have to be revised if the elastic transmission in the system is significantly less than its ideal ballistic value, as, for instance, in the case of inelastic electron tunnelling spectroscopy [15, 16]. In that case, the states $\{|\psi_2\rangle\}$ describe electrons which

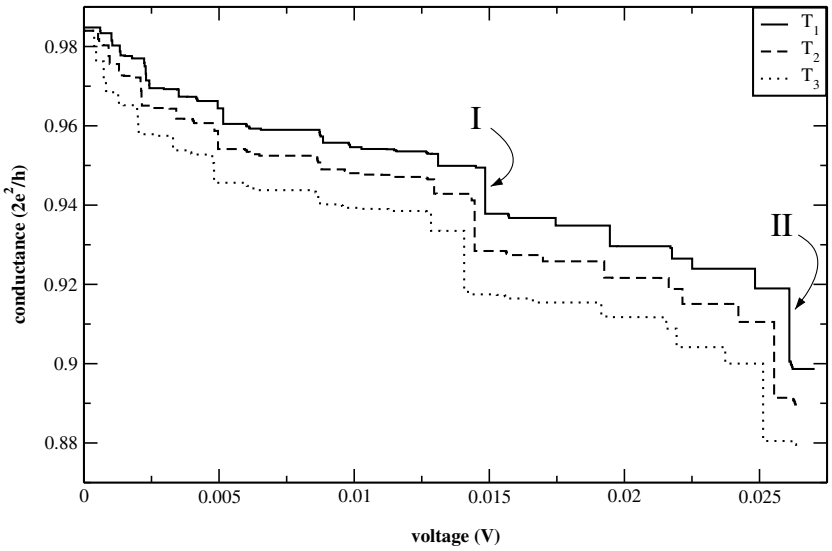

Figure 2. Inelastic differential conductance for the nine-atom chain junction from figure 1 at tensions of $T_1 = 0.48$ eV Å^{-1} (solid curve), $T_2 = 0.56$ eV Å^{-1} (dashed curve) and $T_3 = 0.68$ eV Å^{-1} (dotted curve). The overall elongation applied to the system is 0.09 Å in going from tension T_1 to T_2, and 0.07 Å from T_2 to T_3.

undergo elastic scattering in the nanojunction and which, therefore, emerge partly on the left and partly on the right of the junction. Thus, the inelastically scattered electrons from states $\{|\psi_1\rangle\}$ into states $\{|\psi_2\rangle\}$ are then further divided between the two electrodes, so that δJ in equation (23) is then not the same as the inelastically backscattered current reaching the left-hand electrode. This may be seen by considering the limit where the elastic transmission across the junction is vanishingly small. Then the states $\{|\psi_1\rangle\}$ are almost entirely contained on the left, and the states $\{|\psi_2\rangle\}$ on the right. In that limit, therefore, the inelastically induced current δJ in equation (23) actually provides an additional mechanism for moving electrons from left to right, resulting in an effective increase in conductance.

In the present study, however, we are interested in the ballistic limit, described by equation (24). We see from that equation that σ as a function of W consists of a series of drops. Each drop corresponds to a particular phonon mode, j, and occurs when $eW = \hbar\omega_j$. Physically, as was stated earlier, each conductance drop reflects the increase in resistance that takes place as the respective electron–phonon scattering channel is activated.

3. Results and discussion

Figure 2 shows the differential conductance of the nine-atom chain geometry from figure 1 at three different tensions. At each tension, we see two principal conductance drops, labelled as I and II on the plot. Figure 3 shows a plot of the phonon modes that are responsible for these two dominant conductance drops. We will refer to the mode in the top plot, which corresponds to conductance feature I, as mode I, and to the other mode as mode II. The modes in figure 3 are for the lowest tension but the corresponding modes for the other two tensions are essentially the same. Let us first consider the qualitative features of these results. We see that both modes in figure 3 are longitudinal, at least within the chain. The reason for this may be seen from equations (17) and (18). In any one-dimensional structure with uniaxial

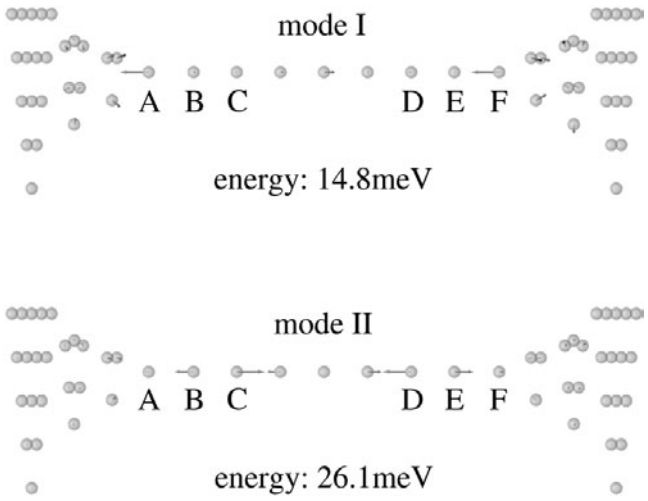

Figure 3. The phonon modes responsible for conductance drops I (top plot) and II (bottom plot) for tension $T_1 = 0.48$ eV Å^{-1} in figure 2.

symmetry, such as the chain, the electron Hamiltonian is stationary with respect to small transverse displacements of the atoms. Hence, the only non-vanishing terms in equation (17) are ones that involve longitudinal atomic displacements: in a linear one-dimensional chain electrons can only couple to longitudinal vibrations.

Let us now consider the nature of the phonon modes in figure 3. Mode I is an Einstein-like, localized vibration involving primarily the two end atoms in the chain, atoms A and F. In mode II, the dominant displacements are those of atoms B and C, and D and E. Therefore, mode II may be thought of as a dimer-like vibration involving the second and second-to-last chain bond, bonds BC and DE. This view of mode II is not unique. For example, one might also think of mode II as a standing wave with a wavelength of eight-thirds of a bond length. However, especially in view of the special properties of bonds BC and DE discussed below, we believe that the dimer-like picture of mode II is, physically, an accurate one and we will continue to employ it in the rest of the paper.

Insight into the origin of these modes may be gained by inspecting the elements of the dynamical response matrix. Figure 4 shows these matrix elements, in magnitude, for the nearest-neighbour bonds in the chain[3]. The actual nearest-neighbour dynamical matrix elements are negative numbers, reflecting the fact that if an atom is displaced, its nearest neighbours experience forces pushing them in the same direction as the displaced atom. Figure 4 shows that, in agreement with previous calculations [2], the first and last bonds within the chain are by far the weakest in the system, whereas the second and second-to-last chain bonds are the strongest. This follows from a general property of metallic bonding:

[3] It must be appreciated that although the tight-binding Hamiltonian is short ranged [2, 4, 5], the resultant force constants are not. The force constants that appear in the matrix $\boldsymbol{K}$ are second derivatives of the energy of the system. They contain long-ranged contributions that arise from gradients of the density matrix. The lower the dimensionality of the system, the more long-ranged the effect of perturbations in the Hamiltonian on the density matrix. For instance, the Hamiltonian in the chain extends only to first neighbours, but the elements of $\boldsymbol{K}$ between second-nearest neighbours in the chain can be as large, in magnitude, as 30% of the nearest-neighbour elements. For qualitative purposes, as in the discussion in connection with figure 4, it can be conceptually useful to think in terms of the nearest-neighbour elements of $\boldsymbol{K}$, and to interpret these elements as effective pairwise springs between atoms. But one must not forget that in reality this is a simplification. For instance, in the numerical calculation of the phonon modes it is necessary to include the full long-ranged structure of $\boldsymbol{K}$, as is done here.

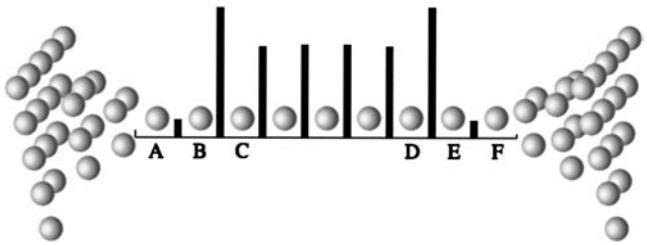

Figure 4. The nearest-neighbour longitudinal dynamical matrix elements, proportional to the length of the bar, for bonds in the chain from figure 1, under a tension of $T_1 = 0.48$ eV Å^{-1}. The longest bar corresponds to a dynamical matrix element of -10.6 eV Å^{-2}.

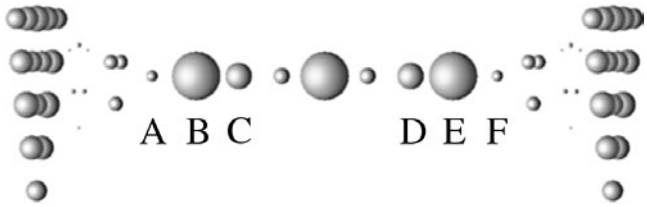

Figure 5. The electronic local density of states at each site in the system from figure 1, under a tension of $T_1 = 0.48$ eV Å^{-1}. The local density of states is proportional to the radius of the circle. The largest circle on the plot corresponds to a local density of states, excluding spin degeneracy, of 0.084 eV^{-1}.

bond strength increases with decreasing coordination number [2]. Atoms A and F have four neighbours each, making their bonds weaker than any other bond in the chain. As a result, during relaxation bonds AB and EF stretch, which further increases the relative strength of bonds BC and DE.

One may thus think of the two end atoms in the chain, A and F, as being the most loosely bound atoms in the system. The Einstein-like phonon mode in the top plot in figure 3 can, accordingly, be thought of as a localized low-frequency rattle of these loosely bound atoms in their respective cages. The reason why electrons couple to this mode strongly, as reflected by the large resulting conductance drop in figure 2, is the large zero-point vibrational amplitude that goes with the low frequency of this floppy mode, and the large resultant electron–phonon scattering cross-section. Mode II in figure 3, on the other hand, is a high-frequency dimer-like vibration of the two strongest bonds in the system, BC and DE. The reason why electrons couple strongly to this mode may be seen by inspecting the local electronic density of states, shown in figure 5. Bonds BC and DE are strong not only from the point of view of the phonons, but also from that of the electrons. An enhanced bond strength results in a reduced bond length, which in turn results in an enhanced electronic Hamiltonian matrix element for the bond. Thus, the two strong bonds, each sandwiched between a pair of weaker ones, act as local resonant traps for electrons. Electrons, accordingly, tend to spend an increased length of time in the strong bonds, BC and DE. This is reflected in the increased local density of states at atoms B and C, and D and E. The enhanced residence time for electrons in bonds BC and DE raises the local electron–phonon scattering rates [3]. Thus, phonon mode II, localized in these very bonds, finds a lively response from the electrons, giving rise to the substantial conductance feature in figure 2. We have repeated the calculation for a chain of length eight atoms. We have found that the main conductance drops are located at similar voltages to those of drops I and II in figure 2. The corresponding phonon modes once again are an Einstein-like mode

involving the two end atoms in the chain and a mode involving dimer-like vibrations in the two strongest chain bonds. A difference from the nine-atom chain is the appearance of slightly more pronounced conductance jumps at intermediate voltages in the eight-atom case, as well as a lower overall conductance (about $0.7\ 2e^2/h$).

By symmetry, one would expect that in addition to phonon mode I in figure 3, there would be a phonon mode, nearly degenerate in energy, with the two end atoms in the chain vibrating in antiphase. Similarly, one would expect there to be a phonon mode, nearly degenerate with mode II, but with the two strong dimers vibrating in antiphase. Indeed, these degenerate modes are present in each case. It might then seem puzzling that, out of such nearly degenerate pairs of modes, only one would show up in a significant way on the conductance curve. To see how that might happen, take, as a simplified example, an infinite linear atomic chain with just two perturbed bonds a distance x apart. Consider the two cases where these bonds are perturbed by the same amount in the same sense or by the same amount in opposite senses. Consider the matrix element for scattering between plane-wave electron states with opposite momenta in each of these two cases. It is not hard to see that these matrix elements would differ from each other by a factor of $[1+\exp(2\mathrm{i}kx)]/[1-\exp(2\mathrm{i}kx)]$, where k is the electron wavevector. Therefore, depending on the values of k and x, electrons may couple preferentially to one of these two realizations of the perturbation. In our case, the electron wavefunctions near the chain ends may be expected to be more complicated than simple plane waves, but the point remains. Indeed, in the case of the eight-atom chain, the Einstein-like mode responsible for the analogue of conductance drop I has the end atoms in antiphase, and the mode for the analogue of drop II has the two strong dimers in antiphase.

Let us now consider the quantitative aspects of the conductance curves in figure 2. Each of the two dominant conductance drops, I and II, shifts down in voltage with increasing tension. Increasing tension results in a reduction in bond stiffness, and hence in a reduction in phonon frequency. Hence, via equation (24), the voltage at which each conductance drop occurs decreases with increasing tension. The reduction in phonon frequency with increasing tension results in an increase in the zero-point vibrational amplitude for each phonon mode. The increased electron–phonon scattering cross-section may be expected to cause an increase in the size of the corresponding conductance drop. Qualitatively, this may also be seen from the factors of $1/\sqrt{\omega_j}$ in the electron–phonon coupling term given in equation (19)[4]. This effect is clearly visible in the case of conductance drop I in figure 2. The corresponding phonon mode, mode I in figure 3, once again, involves the floppiest bonds in the system, which is where the strain may be expected to be localized.

A limitation of the present calculations is the use of a finite submatrix of the full, infinite dynamical response matrix for the electrode–junction–electrode system. This produces a finite set of discrete phonon modes and hence a set of discrete conductance drops, as in figure 2. To overcome this limitation, one must allow the junction phonons to be coupled to the continua of phonon modes in the adjoining electrodes, producing a continuous set of global phonon modes for the electrode–junction–electrode system. The summations over j in equations (23) and (24) would then be replaced by appropriate integrals over phonon frequency, and the differential conductance curve in figure 2 would change its character from being step-wise to being continuous. Such improved calculations will not be considered in the present paper, except to note the following points. As we have seen, the great variation in the effective

[4] The precise functional dependence of the magnitude of the jump on phonon frequency (or, equivalently, on voltage) is difficult to gauge in a simple way, however. While the dominant dependence can be understood in terms of the factor of $1/\sqrt{\omega_j}$ in equation (19), the size of the conductance drops in equation (24) will have a further weak dependence on elongation due to the fact that both the hopping integrals and the electronic Green function in the relaxed structure will vary, albeit weakly, with strain.

spring constant along the chain makes chain phonons quasi-bound resonances, localized in different parts of the chain. Two examples of such localized chain phonons are modes I and II in figure 3: atoms in the domelike contacts on either side of the chain are hardly involved in these modes. The two weak end bonds in the chain act as a double barrier for phonons, leading to the formation of a set of additional quasi-bound phonon resonances in the intermediate section of the chain. Like any resonant wave phenomenon, these quasi-bound chain phonons would be very sensitive to any additional scattering in the system. Hence, in opening the junction to the phonon banks in the reservoirs, it would be essential to ensure that no artificial phonon scattering is introduced at the junction–electrode interfaces, such as might result from an injudicious choice of model for phonons in the electrodes and their coupling to the junction. Beyond that, we expect that opening the junction phonons to the electrodes would get rid of the steplike nature of the conductance curves in figure 2, but would otherwise preserve the shape of the curve. In particular, in view of the high degree of localization of phonon modes I and II in the chain, we expect any broadening of conductance features I and II to be small.

Recently, the inelastic current–voltage characteristics of atomic Au chains have been measured experimentally [6, 7]. There is both significant agreement and significant disagreement between the experimental measurements and the present results. Experiment shows a single dominant conductance drop. This drop agrees well with our drop I in figure 2, both in energy and in its response to elongation of the junction. The disagreement with the present results is that the conductance drop in experiment has a significant energy width, 5–10 meV, and there is no sign, experimentally, of our conductance drop II. There are two possibilities: either drop II does not occur at all in experiment or it is not resolved. It is possible that in experiment the change in dimensionality from the electrodes into the chain is gentler than in the geometry in figure 1. For example, especially under high tension, a distortion in the domelike contacts adjoining the chain could create a situation where the chain is effectively bonded to just two, rather than three, contact atoms. Under a more gradual change in dimensionality, one would expect the variation in bond strength along the chain to be suppressed, with bonds AB and EF stronger, and BC and DE weaker, than at present. That would have the simultaneous effects of bringing phonon modes I and II from figure 3 closer in energy and of making them less localized spatially, and thus broader in energy[5]. Therefore, one possible explanation is that the experimentally observed single broad conductance drop is in fact an unresolved agglomeration of our drops I and II. Another possible explanation is that the chain of Au atoms is a zig-zag arrangement, as suggested by recent density functional calculations [17]. Conductance drop I would still occur at about the same voltage because the end atoms of the chain would still be the most weakly bound. However, at higher voltages, in the zig-zag structure, transverse modes might be excited in addition to longitudinal ones. As a result of this relaxation of the selection rule that restricts excitations to longitudinal modes in our straight chains, in the zig-zag structure conductance drop II may be lost in a host of additional excitations and thus not seen experimentally. A definitive resolution of the question of what happens to drop II in experiment requires more work.

4. Summary

The bond strengths, and the corresponding effective spring constants, vary greatly in a chain junction such as that in figure 1. As is argued above, as well as in [2], this results from the relation between coordination number and bond strength in metallic bonding. Therefore, we do not expect the above results to change in a qualitative way with the details of the electronic

[5] We are grateful to Jan van Ruitenbeek for suggesting this line of thought.

model. The dramatic variation in the dynamical matrix elements shown in figure 4 indicates that it is not appropriate to think of phonons in the chain as free waves. Instead, they are more accurately described as quasi-bound resonances, localized in various parts of the chain. The factors that determine which of these phonon modes couple most strongly to the electrons are to be sought in the specific local nature of the phonons and in the local electronic structure. Thus, as argued above, electrons couple strongly to mode I in figure 3 because of the large vibrational amplitude of that mode, whereas mode II couples well to the electrons because of the enhanced local electronic density of states. We have been able to reproduce the experimentally observed inelastic current–voltage spectral feature, reported in [6, 7], and to capture both its energy and its response to tension. Further investigation would be necessary to determine whether our second main conductance feature, drop II in figure 2, is altogether absent in experiment (and if so why), or is not resolved, as was speculated above.

Acknowledgments

We are grateful to DEL and EPSRC for support through an advanced fellowship and through grant number GR/R36077. We have benefited from many discussions with Jan van Ruitenbeek.

References

[1] Jansen A G M, van Gelder A P and Wyder P 1980 *J. Phys. C: Solid State Phys.* **13** 6073
[2] Todorov T N, Hoekstra J and Sutton A P 2001 *Phys. Rev. Lett.* **86** 3606
[3] Montgomery M J, Todorov T N and Sutton A P 2002 *J. Phys.: Condens. Matter* **14** 5377
[4] Todorov T N, Hoekstra J and Sutton A P 2000 *Phil. Mag.* B **80** 421
[5] Sutton A P, Todorov T N, Cawkwell M J and Hoekstra J 2001 *Phil. Mag.* A **81** 1833
[6] Agraït N, Untiedt C, Rubio-Bollinger G and Vieira S 2002 *Chem. Phys.* **281** 231
[7] Agraït N, Untiedt C, Rubio-Bollinger G and Vieira S 2002 *Phys. Rev. Lett.* **88** 216803
[8] Rubio-Bollinger G, Bahn S R, Agraït N, Jacobsen K W and Vieira S 2001 *Phys. Rev. Lett.* **87** 026101
[9] Todorov T N, Briggs G A D and Sutton A P 1993 *J. Phys.: Condens. Matter* **5** 2389
[10] Todorov T N 2002 *J. Phys.: Condens. Matter* **14** 3049
[11] Todorov T N 1999 *Phil. Mag.* B **79** 1577
[12] Todorov T N 1998 *Phil. Mag.* B **77** 965
[13] Todorov T N 2001 *J. Phys.: Condens. Matter* **13** 10125
[14] Todorov T N 2000 *J. Phys.: Condens. Matter* **12** 8995
[15] Jaklevic R C and Lambe J 1966 *Phys. Rev. Lett.* **17** 1139
[16] Stipe B C, Rezaei M A and Ho W 1998 *Science* **280** 1732
[17] Sanchez-Portal D, Artacho E, Junquera J, Ordejon P, Garcia A and Soler J M 1999 *Phys. Rev. Lett.* **83** 3884